

# Automatic age interpretation of cod otoliths using deep learning

Endre Moen<sup>1\*</sup>, Rune Vabø<sup>1</sup>, Szymon Smoliński<sup>2</sup>, Côme Denechaud<sup>1</sup>, Nils Olav Handegard<sup>1</sup>, Ketil Malde<sup>1,3</sup>,

**1** Institute of Marine Research, Bergen, Norway

**2** Department of Fisheries Resources, National Marine Fisheries Research Institute,  
Kołłątaja 1, 81-332 Gdynia, Poland

**3** Department of Informatics, University of Bergen, Norway

\* endre.moen@hi.no

## Abstract

The age structure of fish populations is a central input in stock management, and a valuable data in most biological studies. Fish age can be inferred by counting annual increments in otoliths. Typically, fish age is estimated manually by experts by visual interpretation of otolith structures, but this process is time and resource-consuming. In this study, we develop a machine learning framework for automating the age estimation of Atlantic cod (*Gadus morhua*) based on multi-exposure images of broken otoliths (N= 5150). We apply the two architectures (EfficientNetV1 and EfficientNetV2) using three and two different model sizes from each family, comparing the performance of different models and their ensembles. The average accuracy of the 17 tested models was 72.7% and the average MSE was 0.284. The models' accuracy for one and two years old individuals was over 90% and no systematic bias in the age predictions across age groups was observed. Models EfficientNet B4 and EfficientNet B6 with the lowest image exposure were the top-scoring models. After an exhaustive search, a maximum accuracy of 78.6% was achieved with an ensemble consisting of six models. The tested models strongly correlate in terms of predictions. Variations in percentage agreement between

age classes showed similar patterns in both CNN-based predictions and human readers,  
17 with generally decreasing agreement with age. While percentage agreement from  
18 CNN-based predictions was often lower than for human experts, it remained within or  
19 close to the range of percentage agreement observed across readers. Our results  
20 demonstrate that the use of deep learning techniques in the analysis of otoliths has  
21 potential for facilitating automation. When developing the framework for automatic age  
22 estimation, we recommend including B4 architectures as they are quick to train and  
23 perform well. Ensemble approaches are also recommended if sufficient computational  
24 resources are available, as they can give increased accuracy and lower variance of the  
25 predictions. We find that under-exposed images tend to perform better than other  
26 exposures. Our study can serve as a baseline for the future development and  
27 operationalization of CNN models and the inclusion of automatic otolith-based age  
28 interpretations in the biological data collection routines. In contrast to previous studies  
29 trained on otolith sections requiring a time-consuming preparation, we used broken  
30 otoliths that require no processing before imaging. This shows the potential for more  
31 resource-efficient training framework providing near *at-sea* age estimates.  
32

## Introduction

33

Knowledge of fish age structure is central to the study of fish and stock dynamics. It  
34 informs on population growth and mortality and is one of the main criteria used for  
35 determining the health of exploited populations and monitoring the effects of selective  
36 fishing (Hidalgo et al., 2011; Brunel and Piet, 2013). Changes in the age distribution  
37 can track significant changes in population structure, such as the appearance of a  
38 particularly strong year-class (Reglero and Mosegaard, 2006), or the gradual truncation  
39 of older age classes as selective fishing mortality removes larger individuals (Siskey  
40 et al., 2016). Hard structures such as scales and otoliths are used worldwide as one of  
41 the primary sources of fish age estimates, due to their ability as natural physiological  
42 and environmental recorders to form regular, temporally resolved growth increments at  
43 the annual levels (Campana, 2001; Francis and Campana, 2011; Albuquerque et al.,  
44 2019). While age is inferred from the “simple” counting of annual increments, the  
45 interpretation of this zonation pattern is species or even population-specific (Høie et al.,  
46

2009) and is based on precise knowledge of the timing of zone formation and of the  
correct identification of true and false zones (Panfili et al., 2002). This process, therefore,  
requires specific expertise and is subject to uncertainties in both between-reader  
precision and “true” age accuracy (Francis and Campana, 2011). Therefore,  
streamlining, scaling, and increasing the quality of age estimations can improve the  
reliability of evaluations of fish biology and consequently assessment of stock size and  
structure (Tyler et al., 1989; Beamish and McFarlane, 1995; Ragonese, 2018).

Otolith reading is time and resource-consuming. Training of expert readers can take  
several years depending on the species, and otoliths often undergo a long processing  
phase before the final age estimates can be produced (Carbonara and Follesa, 2019).  
This is particularly true for demersal fish species, like Atlantic cod (*Gadus morhua*),  
that have large opaque otoliths that typically require time-consuming preparation  
(Denechaud et al., 2020; Smoliński et al., 2020). These routines vary between  
populations and institutes and range from a direct reading of broken otoliths under a  
magnifying glass, to embedding, thin sectioning, and finally imaging of the sections  
under a microscope. There has been a variety of methods proposed to automatically  
interpret otoliths, which range from one-dimensional data analysis like intensity  
transects (Mahé, 2009) to the more recent effort toward developing machine learning  
(ML) frameworks (Moen et al., 2018; Politikos et al., 2021).

## About deep learning and image analysis

During the last decade, deep learning has become one of the dominating fields of  
machine learning where various architectures of deep neural networks are able to learn  
to efficiently and identify patterns and structures in various types of data (LeCun et al.,  
2015). Within the field of computer vision, deep Convolutional Neural Networks (CNN)  
have been widespread ever since (Krizhevsky et al., 2012) won the annual ImageNet  
Large Scale Visual Recognition Challenge (ILSVRC) competition (Russakovsky et al.,  
2014). ILSVRC remains the most important benchmark for image classification with 1.4  
million images in the ImageNet training set, and state-of-the-art CNNs are therefore  
often targeted to this data set. Many of these CNNs are publicly available including  
their trained network weights. It is therefore often useful to use transfer learning with

these pre-trained weights as a starting point. This is especially true for tasks where relatively little training data is available. For many fish species, age estimation from images of otoliths represents precisely such a task. InceptionV3 (Szegedy et al., 2015) was modified to predict the age of Greenland halibut (*Reinhardtius hippoglossoides*) from otolith images (Moen et al., 2018), and a modified InceptionV3 was applied to classify otolith images of red mullet (*Mullus barbatus*) (Politikos et al., 2021). While some state-of-the-art CNNs grew in model size a recent CNN architecture called EfficientNet (Tan and Le, 2019) demonstrated that increased performance could be achieved with smaller model sizes (number of parameters) using a compound scaling method for network depth, width and image size, resulting in a family of seven different models with different sizes. This network has been successfully applied with transfer learning to analyse images of salmon scales (Vabø et al., 2021). Recently a successor to the EfficientNet architecture, EfficientNetV2 (Mingxing Tan and, 2021), has been made available.

In this study, we develop a learning framework for automating the age estimation of Atlantic cod based on multi-exposure images of broken otoliths. We apply the two EfficientNet family architectures EfficientNetV1 and EfficientNetV2 using three and two different model sizes from each family respectively. We compare the performance of the different models and discuss the use of an ensemble of models to improve estimation accuracy. Our study identifies specific features of investigated architectures and suggests the best practices and strategies to develop CNN frameworks for the predictions of the age of fish based on otoliths. It can serve as a baseline for the future operationalization of CNN models and the inclusion of automatic otolith-based age interpretations in the biological data collection routines.

## Method and materials

### Data Collection

We used a data set sampled from 5150 cod otoliths collected on surveys conducted by the Institute of Marine Research (IMR) in the period 2012-2018 and aged by otolith experts. On each of the surveys, the otoliths were sampled using a random-stratified

sampling based on fish length for each trawl station.

106  
Each otolith was broken in the transverse plane and placed on a mount before it was  
107 captured by six images with three light exposures and one rotation of  $180^\circ$  (Figure 1).  
108 The images were taken with a resolution of  $3744 \times 5616$  pixels. The image light exposure  
109 punctually varied depending on light conditions coming from outside. Light exposure  
110 was stored in the metadata of the JPG file. Details can be found in (Myers et al., 2019)  
111 and in the data set available at <https://doi.org/10.21335/NMDC-1826273218>.  
112

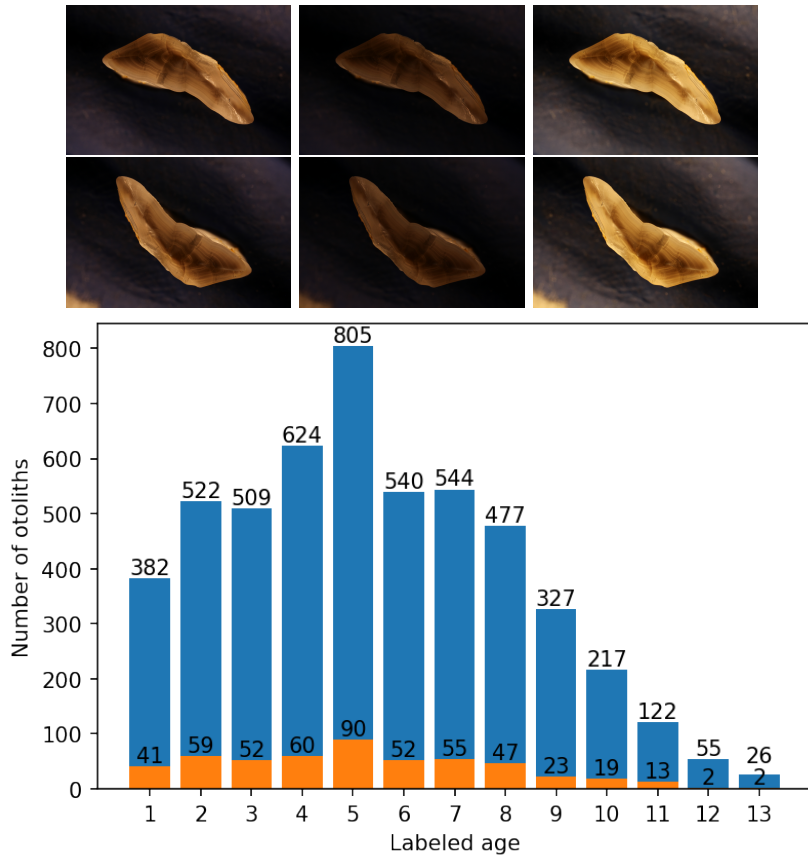


**Figure 1.** Images of an otolith collected in 2016 from a 6 years old cod (top), taken with medium-, minimum- and max-exposures (upper row), then rotated  $180^\circ$  (lower row). The age distribution of the 5150 otoliths in the training (blue), and the 515 otoliths in the test (orange) set (bottom).

## Convolutional neural network architecture

113  
Each CNN was trained using transfer learning by loading ImageNet weights. The  
114 training images were resized from  $3744 \times 5616$  pixels to between  $380 \times 380$  and  $528 \times 528$   
115 pixels depending on the architecture. The pixel values have a range between 0 and 255,  
116

which was normalized to between 0 and 1. Test set predictions were done on images  
117  
resized to  $380 \times 380$  and  $384 \times 384$  pixels. To investigate the effect of exposure and  
118  
orientation as presented in the image-taking protocol described in (Myers et al., 2019),  
119  
we also trained on 9-channel images by stacking 3 RGB images representing 3 different  
120  
lighting exposures. Using Timm (Wightman, 2019), the ImageNet weights were  
121  
duplicated on the input layer to accommodate 9 channels. The three images used were  
122  
of dark, medium, and light exposure.  
123

CNNs were selected based on performance on the ImageNet benchmark and the  
124  
availability of open-source implementations with pre-trained weights. The CNN models  
125  
are aimed at classification, while we treated aging as a regression problem (Moen et al.,  
126  
2018; Vabø et al., 2021). The last layer of the CNNs was therefore modified to a linear  
127  
output. For the EfficientNetV2 family we did this by applying three multi-layer  
128  
perceptron layers going from 1280 output of the last hidden layer to a dense 256-layer,  
129  
then a leakyRelu (Xu et al., 2015) layer, then a dense 32-layer, then a leakyRelu layer,  
130  
and finally a linear output layer. For EfficientNet we only changed the last layer from  
131  
softmax to a linear output.  
132

To each fold, we normalized the age on the training set by subtracting the mean and  
133  
scaling to unit variance. The normalization was then applied to the validation and test  
134  
sets. Test set predictions were obtained by applying the inverse transform.  
135

## Implementation and training

  
136

EfficientNetV1 B4, B5, and B6 were imported and modified with TensorFlow (Abadi  
137  
et al., 2016) and Keras (Chollet and others, 2018) software packages in Python.  
138  
Computation was done using CUDA 11.1 and CuDNN with Nvidia (Nvidia Corp.,  
139  
Santa Clara, California) A6000 accelerator card with 48 GB of GPU memory and P100  
140  
cards with 12 GB of GPU memory, EfficientNetV2 Medium, and Large were imported  
141  
and modified with the PyTorch (Paszke et al., 2019) and Timm (Wightman, 2019)  
142  
software packages. Computation was done on P100 and RTX 3090 with 24 GB of GPU  
143  
memory. Pretrained weights for EfficientNet were available from Keras, and pre-trained  
144  
weights for EfficientNetV2 were available from Timm. The models will be referred to as  
145  
B4-Min, B4-Middle, B4-Max, B5-Min, Medium-min and so on by combining model  
146

name with image exposure.

Augmentation was applied to the training set. The images were augmented using rotation between 0 and 360 degrees, and reflection by the vertical axis.

The cost function used was mean squared error (MSE) while the metric used for evaluating the models and comparing them to expert readers was accuracy. Accuracy was obtained by rounding the floating point number predictions to the nearest integer and comparing the age classification against the true labels.

The data set of 5150 otoliths was divided into a training set constituting 90% of the otolith images (4635 otoliths) and a test set of 10% (515 otoliths). To get the most out of a small data set we applied 10-fold cross-validation on the training set. This meant that 10% of the training set was used for validation and 90% (81% of the whole data set) was used for the actual training for each fold. Consequently, 10 different models were trained with a different set of 463 images used for validation in each fold, i.e. each data point participates in the validation set once and in the training set 9 times. Among the 10-fold models, the one with the best MSE was chosen. The best model parameters on the validation set were then used to predict the age on the test set, and the metric for accuracy and MSE were recorded. The test set is chosen at random, while the 10-fold split of the training set is chosen using a stratified k-fold split, which preserves a similar distribution of the whole cross-validation set in each validation set. That means the 463 images in the validation set will have similar age distribution to that of the 4635 images in the cross-validation set.

## Hyper-parameters

The CNN hyper-parameters configurations varied a little between the two families of networks, but were kept the same within the families. Some hyper-parameters that were tuned are batch size, learning rate, k-fold size, weight decay, step size, number of epochs, early stopping, and patience. Some parameters are constrained by the GPU memory, like batch size which was set to 16 for models trained on the A6000 card, and to 8 for the models trained on P100s.

EfficientNet used learning-rate with a weight decay scheduler, while EfficientNetV2 used Cosine Annealing scheduler (Loshchilov and Hutter, 2016). The training- and

validation image size used was not changed, except for EfficientNetV2 Large which uses  
177 a smaller validation image size. The exact configuration of each network is available  
178 with each network result on the GitHub page of the project  
179 (<https://github.com/emoen/Deep-learning-for-regression-of-cod-otoliths>). The  
180 hyper-parameters are available in Table 3, and 4 in supplementary information.  
181

## Ensemble learning with averaging

182

Ensemble learning is an algorithm that combines the predictions from multiple models  
183 to reach a final prediction and obtains a predictive performance that is better than any  
184 of the constituent models alone.  
185

We evaluated two types of simple ensemble averages. The first ensemble was the  
186 average of the 10-fold cross-validation, which was reported as the model performance.  
187 This ensemble of 10 model weights was reported as one model because the architecture  
188 and image exposure was the same. Only the training and validation data were different  
189 in these models. The model weights were selected during training when the model had  
190 the lowest MSE on the validation set. The average MSE and accuracy of the prediction  
191 of the 515 test images from 10 folds on the test set were reported as the model MSE,  
192 and accuracy.  
193

The second ensemble was created from selections consisting of 2, 3, 4 models, and so  
194 on up to an ensemble containing all 17 models. These ensembles combine 20, 30 and up  
195 to 170 predictions on the test set. The accuracy was reported after rounding.  
196

## Correlations of predictions on the test set and clustering analysis

197

Correlations of predictions on the test set were investigated by creating a correlation  
198 matrix of each model's prediction of each age class. This matrix showed how much the  
199 models were in agreement, and clustering analysis identified which models were more in  
200 agreement with each other. We used Pearson's correlation coefficient and hierarchical  
201 clustering (HCA) with Euclidean distance and complete linkage.  
202

## Comparison of CNN with human readers

To evaluate the credibility of CNN predictions in relation to human readers, we compared the mean percentage agreement of the test set predictions within each age class with those from multiple human readers from a recent internal cod age reading workshop carried out at the Institute of Marine Research, Norway. In this workshop, a different set of 100 otoliths from Atlantic cod were read by seven readers, of which five were certified advanced cod readers and two were under training. By comparing the results of the test set to the mean agreement and standard deviation of predictions within the age class from the workshop, we evaluated if machine-driven estimates were behaving in line with those anticipated by human readers.

## Results

The mean accuracy of the 17 models was 72.7% (Table 1) on the test-set, and the standard deviation was 1.1. The least accurate model was B4-max with 70.9%, and the most accurate model was B5-min and B6-middle with an accuracy of 74.4%.

B5 was the highest scoring model on all the exposures (min, middle, max) with a mean accuracy of 73.7%, and min-exposure was the best exposure with a mean accuracy of 73.3%. Both B5 and B6 from the EfficientNet family were better than Medium and Large from the EfficientNetV2 family.

The mean MSE of the 17 models was 0.284 on the test set, and the standard deviation was 0.022. The highest MSE was from B5-max with MSE of 0.359, and the lowest MSE was from B6-middle exposure with MSE of 0.262. We find that the differences between models are statistically significant (ANOVA,  $p = 1.6 * 10^{-7}$ ), but that the differences are not significant for the individual factors of model architecture (two-way ANOVA,  $p = 0.139$ ) or image exposure ( $p = 0.057$ ). The interaction plot for two-way ANOVA is shown in Figure 2. See Table 13 in the supplementary information for a T-test of all models.

Medium and Large were the best models with a MSE of 0.278, and the 9-channel composite images gave better results than any individual exposure, with a MSE of 0.272. The high MSE for B5-max and B6-max was due to a large misprediction of the image with index 308 in the test set labeled 1 year and predicted 5.7 years (see Table 7 in

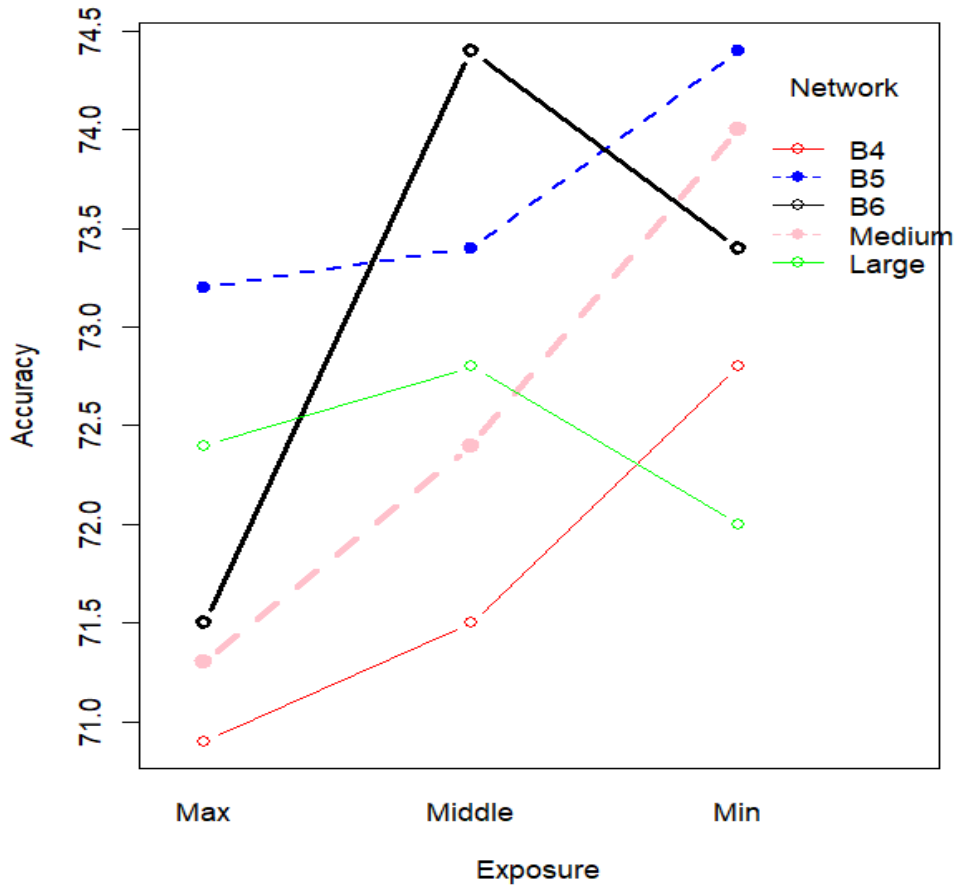


**Figure 2.** Interactive plot of the 5 networks with image exposure on x-axis and ensemble accuracy on the y-axis. We see that under-exposed images perform better for all but the B6 and Large network.

**Table 1.** Mean accuracy, MSE, and Percentage Agreement (PA) on the test-set by light exposure and CNN architectures

Acc:light/CNN	EfficientNet V1			EfficientNet V2		
	B4	B5	B6	Medium	Large	Mean
min	72.8	<b>74.4</b>	73.4	74.0	72.0	73.3
middle	71.5	73.4	<b>74.4</b>	72.4	72.8	72.9
max	70.9	73.2	71.5	71.3	72.4	71.9
9 channels	-	-	-	74.0	72.2	73.1
<b>Mean</b>	<b>71.7</b>	<b>73.7</b>	<b>73.1</b>	<b>72.9</b>	<b>72.4</b>	<b>72.7</b>
MSE:light/CNN						
min	.277	.277	.272	.273	.280	.276
middle	.285	.273	<b>.262</b>	.278	.275	.275
max	.291	.359	.305	.289	.286	.306
9 channels	-	-	-	.273	.271	.272
<b>Mean</b>	<b>.284</b>	<b>.303</b>	<b>.280</b>	<b>.278</b>	<b>.278</b>	<b>.284</b>
PA:light/CNN						
min	89.5	89.3	88.2	89.7	89.9	89.3
middle	88.2	89.5	90.9	91.1	87.8	89.5
max	87.6	90.5	88.0	89.5	90.3	89.2
9 channels	-	-	-	<b>91.3</b>	91.1	91.2
<b>Mean</b>	<b>88.1</b>	<b>89.8</b>	<b>89.0</b>	<b>90.4</b>	<b>89.8</b>	<b>89.6</b>

supplementary information on outliers).

Medium-all was the highest scoring model with percentage agreement (PA) 91.3%  
233  
and B4-max was the lowest scoring model with PA 87.6% (Table 1). Medium was the  
234  
overall best performing model and B4 was the worst. The 9-channel composite images  
235  
outperformed individual exposures, while max exposure had inferior performance to the  
236  
others.  
237

When comparing each 10-fold ensemble average prediction accuracy, and MSE for all  
238  
17 models, the ensemble metric was either better than or in the upper quantile for all  
239  
the models (Figure 3). The prediction MSE and accuracy of each fold are given in  
240  
supplementary information (Table 5, 6).  
241

## Prediction by age class

When calculating the accuracy of all models by age class, we found that accuracy for  
242  
one- and two-year-olds was better than 90% (supplementary information in Figure 9).  
243  
All age classes six years or younger were correctly classified with more than 70%  
244  
accuracy, and all 13-year-olds were predicted to be younger.  
245

No systematic bias in the age prediction of CNN is visible except for the  
246  
underestimated age of individuals aged by the expert reader as 13 years old (Figure 4).  
247

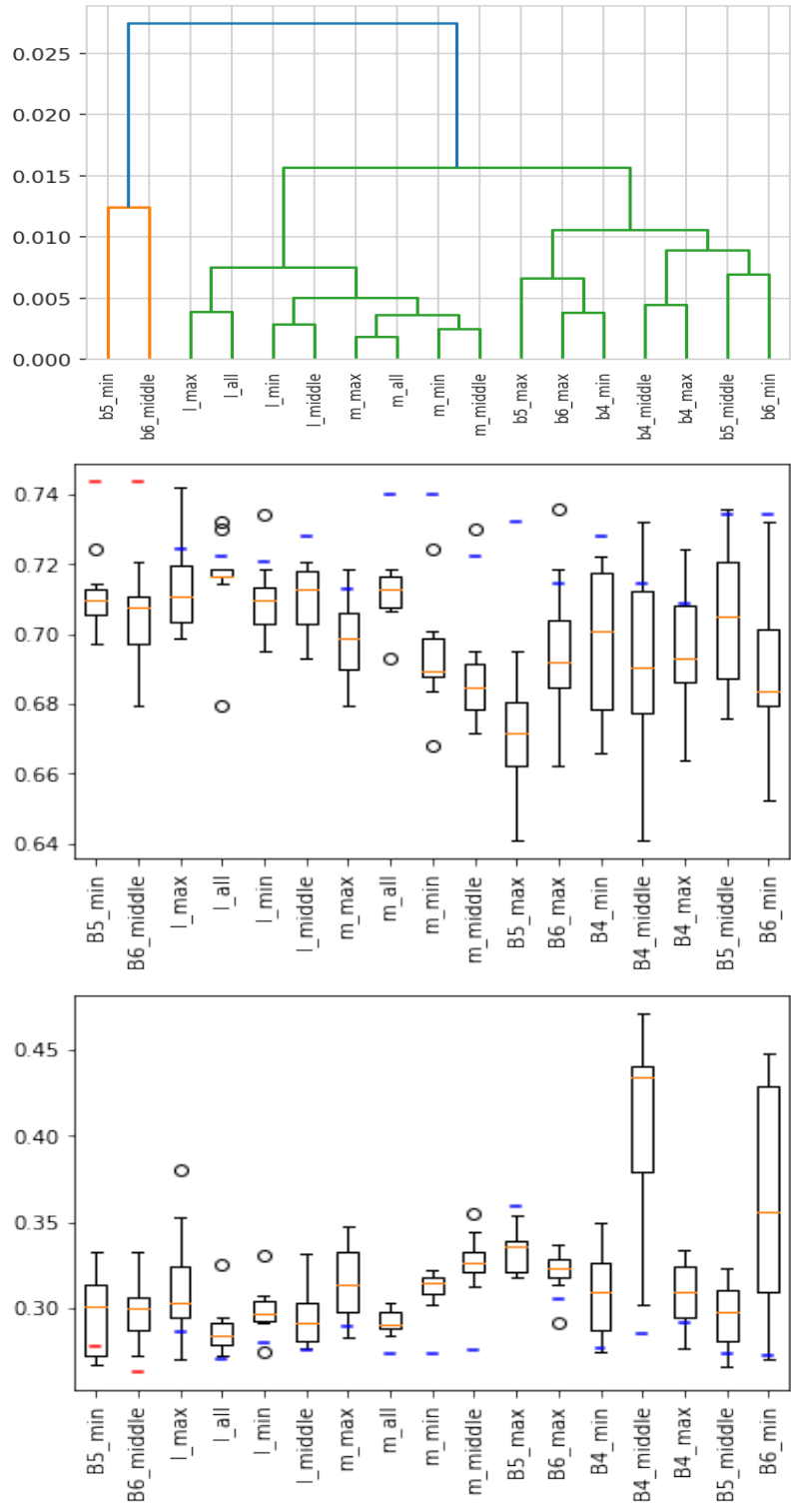


**Figure 3.** Hierarchical clustering (HCA) on the correlation of predictions (top), a box-plot of accuracy score (middle), and MSE (bottom) of all the 17 models. In (middle) and (bottom), the blue line is ensemble-average prediction accuracy (or MSE) on the test set, the red lines are the two best ensemble-average predictions on the accuracy, and the orange lines are the mean of the 10-fold predictions.

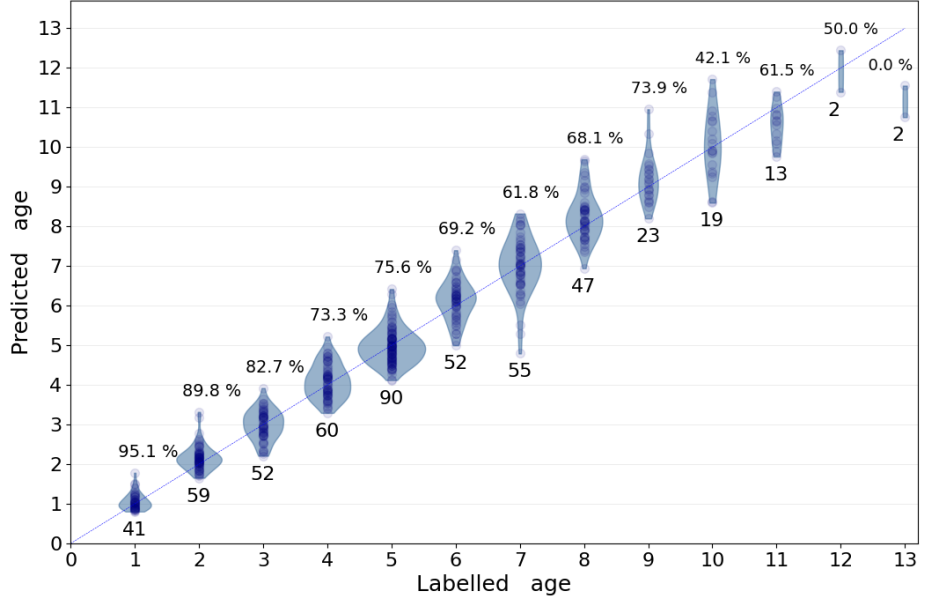


**Figure 4.** Violin plot of predicted age from model B5-min with accuracy of 74.4%. Above each age is the accuracy, and below is the total number of images in the test set of that age class

### Simple ensemble-average predictions

We searched the space of ensembles-average predictions of 2 to 17 models, which is the set of unordered combinations without replacement, equal to the binomial coefficient  $\sum_{k=1}^N \binom{N}{k}$  where  $N = 17$  and  $k \in 2..N$ . For each set of ensemble combinations, we recorded the best ensemble and found that the best overall ensemble prediction was an ensemble of six models which produced an accuracy of 78.6%. The ensemble consisted of B4-min, B5-min, B6-min, Medium-min, B6-middle, and B4-max. The results are presented in supplementary information in Table 10, 11, and 12.

The ensemble accuracy decreased after adding 6 models, while the MSE continued to decrease until all 17 models were included. This was as expected from the theory on simple ensemble average learning since the variance is reduced with more models.

We observe that model B4-min (No 1), and B6-min (No 3) were the most often present in the top scoring model with inclusion in 14 ensembles (Table 2). These models did not have the highest accuracy (B5-min, and B6-middle) but an accuracy of 72.8%

**Table 2.** Rank statistics of models by participation in the best ensemble of size 1 to 17 when the loss function is accuracy.

Rank	Model name	Count
1	B4_min	15
1	B6_min	15
3	B5_min	13
3	M_min	13
5	B6_mid	12
6	B5_mid	10
6	B4_max	10
8	L_mid	9
9	B6_max	8
10	M_mid	7
10	M_all	7
10	L_all	7
13	M_max	6
14	L_min	5
14	B4_mid	5
14	B5_max	5
14	L_max	5

and 73.4%. This was lower than the highest accuracy models, which were B5-min and B6-middle (74.6%) with a rank of 3 and 5 respectively.

The mean ranking by exposure types was: min-exposure (rank 4.4), middle-exposure (rank 8.6), 9-channel composite (rank 10), and max-exposure (rank 11.2). The mean ranking by architecture was EfficientNet (rank 6.6), and EfficientNetV2 (rank 10.3).

## Outliers

Figure 5 shows 4 images that were incorrectly classified with an error larger than 1 year after rounding. All the images with more than 1 year in prediction error are shown in supplementary information (Table 7), with comments by an expert on the most common mispredictions (Table 8). Large outliers occurred throughout all of the tested models and ensembles in small numbers. Most of those outliers were identified as visually challenging images with artifacts and/or low readability. For example, image 13 was overestimated in all B models, likely due to a clear zone in the inner core region that an expert reader would identify as a settlement false zone and ignore. Similarly, many outliers, such as images 270 and 369, showed multiple narrow false zones in the mid-section of the otolith that were likely to affect age determination. Alternatively, cases such as images 71 and 342 showed clear issues with age interpretation when the

image deviates from the standard of the training set, such as when the exposure was  
282 changed drastically or when break lines interrupted the normal pattern of ring  
283 deposition. In one case (image 362), all models estimated the otolith to be 5 instead of 7  
284 years old: upon visual investigation, the otolith was clearly 5 years old, and the initial  
285 age had likely been misread.  
286

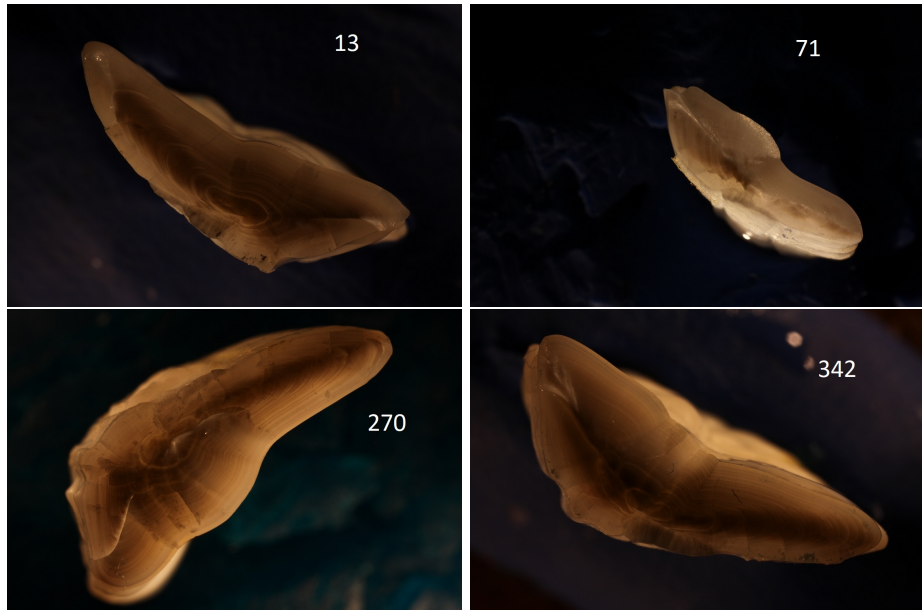


**Figure 5.** Example outlier images with index 13, 71, 279, 342 from the test-set were  
mispredicted by between 25% and 100% of the models

Some cod otoliths were outliers to all models and on all exposures (e.g. otoliths 71,  
287 342, 362, and 369), to a family of models and on all exposures (e.g. otoliths: 13, 423),  
288 to some models and on one exposure (E.g otolith 308), and to both families of models  
289 and on some exposures (E.g. otolith 320).  
290

We also observed that the number of outliers did not correlate with model  
291 performance. *E.g.*, B5-min, and B6-mid which had 7 and 9 outliers, but the best  
292 accuracy. While B4-max with the lowest accuracy (70.9%) had the least number of  
293 outliers with only 6 mispredictions.  
294

### Correlation of predictions and cluster analysis

The correlation of models on the test-set predictions given in Figure 10 in  
296 supplementary information shows that the models strongly correlate in outlier  
297 predictions. The correlation from all the predictions on the test set varied between  
298

0.988 to 0.999, with the lowest correlation found between B5-min and Medium-min. 299

Hierarchical clustering (HCA) of the models found 3 clusters, B5-min, and 300  
B6-middle, which are the two best models, a cluster of all the EfficientNetV2 models, 301  
and a cluster of the rest of the models (Figure 3, and 10). 302

The two least correlated models, B5-min and Medium-min, which had Pearson's 303  
correlation of 0.988 showed strongly correlated predictions also on a sub-year scale 304  
(Figure 6). This means that the model output is not simply a Gaussian or other 305  
symmetric distribution around the correct (integral) value, but that the models identify 306  
characteristics of the input that lead them to classify it to a highly precise fractional 307  
value. 308

## Comparison of CNN with human readers 309

Variations in percentage agreement between age classes showed similar patterns in both 310  
CNN-based predictions and human readers, with generally decreasing agreement with 311  
age (Figure 7). Within each age class, percentage agreement from CNN-based 312  
predictions was lower than the average for multiple human readers and increasingly so 313  
for the older age classes. However, they often remained within or close to the range of 314  
percentage agreement observed across all readers for all otoliths of a given age class. 315

## Discussion 316

### Accuracy across different age groups 317

The age of the younger individuals was predicted with greater accuracy than those of 318  
older individuals by our models. Thus, the CNN appears to be particularly competent 319  
at aging cod otoliths of younger age. This is also typical for expert readers who 320  
generally show the greatest accuracy for the youngest age classes which have fewer and 321  
clearer rings (Campana, 2001). However, the reasons both humans and CNNs find the 322  
age of younger individuals easier to predict may not be the same. Human expert readers 323  
use various visual cues, prior knowledge, and background information to determine fish 324  
age, such as comparing ring counts on multiple axes and having intrinsic knowledge of 325  
the periodicity of opaque and translucent zones for a given species. In younger fish, the 326

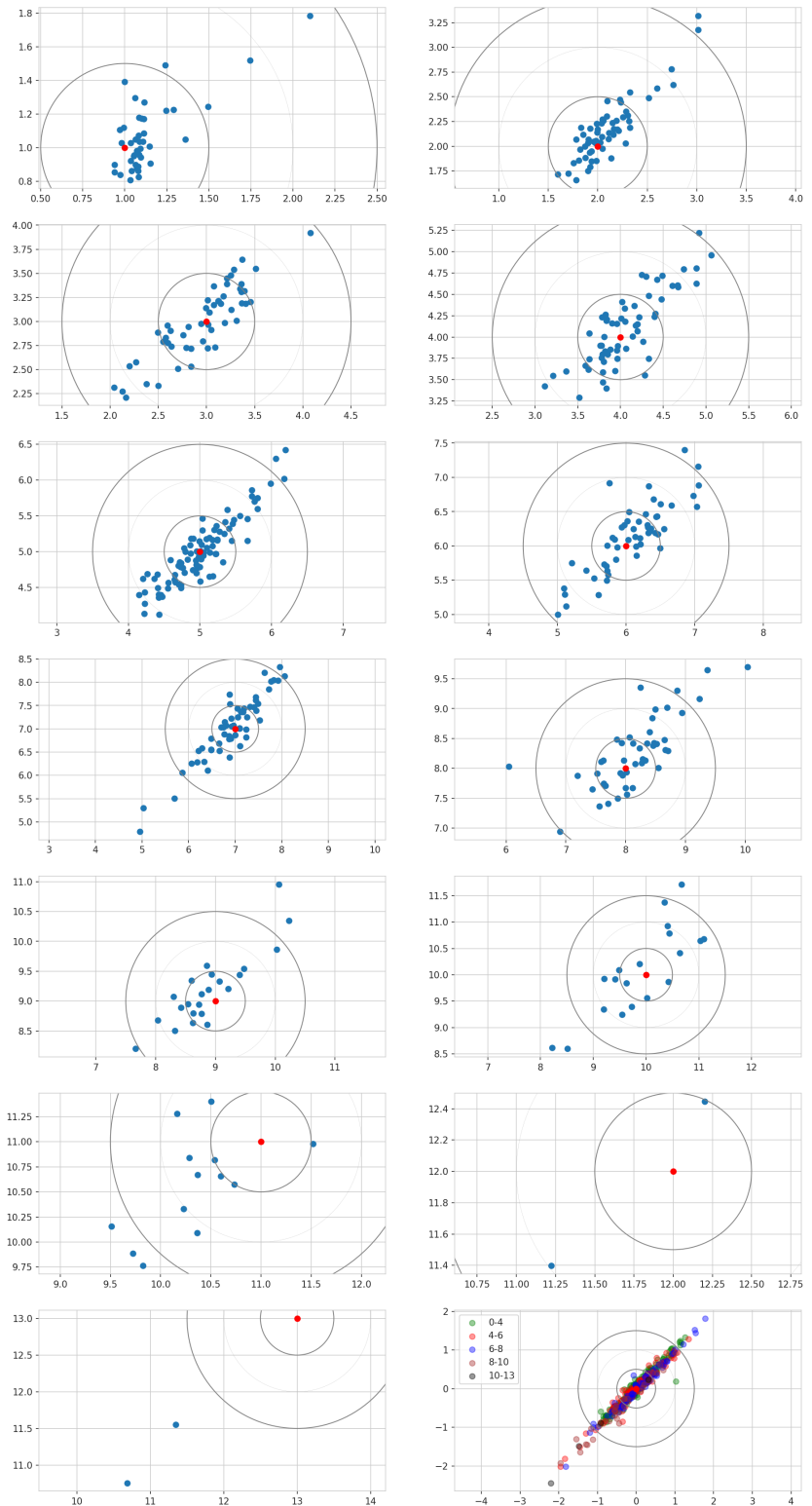


**Figure 6.** Comparison of age estimates predicted by Medium-min (x axis) and B5-min (y axis) as age-specific scatter plots (A to M). Differences with expert reader age aggregated by age group are presented in the last panel (N).

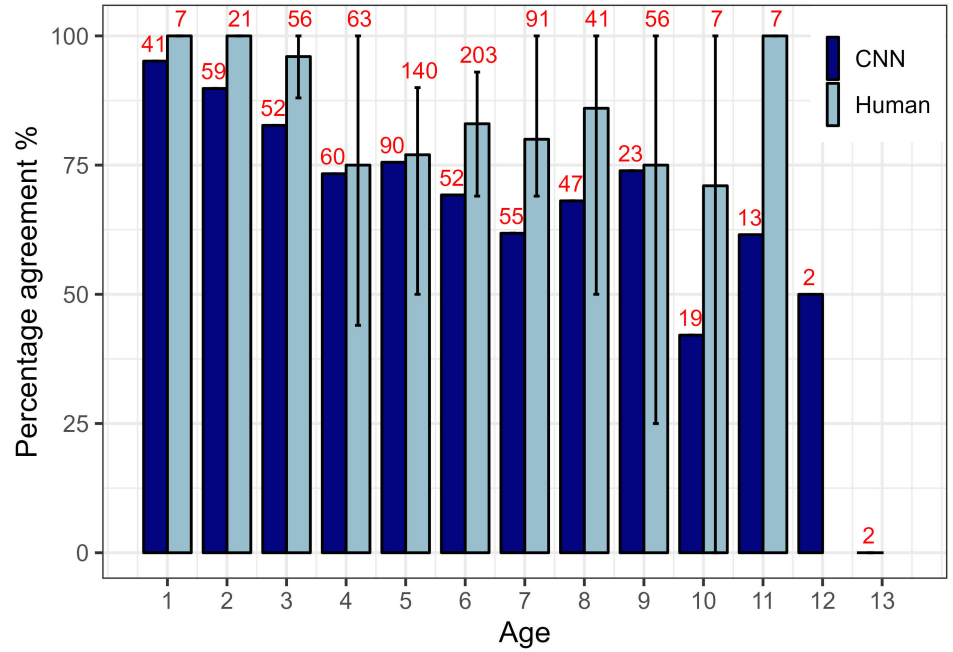


**Figure 7.** Comparison of mean percentage agreement within each age class for two sets of otoliths: the CNN-predictions on the test set (black); an internal age reading of 100 cod otoliths involving 7 readers (gray). Numbers indicate the total number of readings for each age class (with 1 reading per otolith for the CNN but 7 readings for the workshop). Error bars indicate the range of percentage agreement between readers for all otoliths of a given age class.

increments are usually wider and more clearly separated as fish -and consequently  
327  
otolith- growth rates are maximal prior to maturity. Fish of age 1 are small and have  
328  
comparatively small otoliths with a straightforward ring pattern made of one single  
329  
finished opaque and translucent zone, and expert readers are unlikely to disagree on it  
330  
interpretation. On the other hand, a CNN architecture as used here identifies  
331  
hierarchical patterns on different scales of the image from which it derives a value in the  
332  
range of those provided in the training set. This means that unless specifically forced to  
333  
do so, the algorithm may seek and interpret visual clues other than the rings human  
334  
readers are trained to use. A possible explanation for the higher prediction accuracy of  
335  
younger fish is that age is related to the area the otolith covers relative to the total  
336  
image size. Because the same camera settings were used all images had the same  
337  
dimension and calibration. For a species with moderately large adults such as Atlantic  
338  
cod (Froese and Pauly, 2022), the otoliths will grow in size significantly faster during  
339  
the first years and then slow down with approaching sexual maturity. This is especially  
340

marked for the first couple of years where there is likely a more distinct size  
stratification of the otoliths from one year to another. As fish get older different growth  
trajectories will then lead to greater overlap in otolith sizes across different ages. It is  
therefore possible that the CNNs are not counting growth zones as human expert  
readers would, but rather that they synthesize all available patterns in the image to find  
recurring characteristics to the ages provided in the training set. The size of the area  
that the otoliths cover against the more uniform black background might for example be  
a very simple feature picked up by the CNNs yet with high predictive power for the  
youngest fish, while the higher inter-individual variability and greater size overlap at  
older ages would affect the predictive accuracy of CNNs

The hypothesis that CNNs exploit other information than the growth zones is  
consistent with the findings of an earlier study where network activations inside a CNN  
were explored for images of Greenland halibut otoliths (Ordonez et al., 2020).  
Visualisation techniques were used to reveal the relative importance of attributes such  
as shape, inner structure, and size of the otoliths using activation maps. Importantly,  
the authors found that the CNN utilized information in pixels corresponding to annual  
increments to only a small extent.

## Importance of training set size relative to model performance

It is commonly recognized that the performance of deep learning systems often improves  
with more training data(LeCun et al., 2015). A crucial issue in machine learning  
projects is then determining the amount of training data needed to achieve a specific  
performance goal. In this study we utilized a somewhat large data set of around 5000  
images, although the images were divided among a large range of age classes. In  
comparison, it is not uncommon for deep learning systems for image classification such  
as ImageNet to be trained on thousands of images for each class (Russakovsky et al.,  
2014). In this study, the use of transfer learning (Yosinski et al., 2014) and  
augmentation yielded a significant performance boost but it is still likely that the  
network would provide more robust predictions with a larger training set. From a  
preliminary initial training not reported as part of this study, we trained a B4 network  
on about 2000 images and obtained an accuracy of around 60%. When another 3000

images were added to the data set accuracy reached about 70%. This could suggest that  
371  
increasing our sample size would have further increased accuracy.  
372

## The effect of image size 373

The high-resolution  $3744 \times 5616$  cod otolith images were scaled down to between  
374  
 $380 \times 380$  and  $528 \times 528$  pixels to match the requirements of the different EfficientNet  
375  
architectures. This reduction in resolution may have affected the readability of  
376  
finer-scale visual features such as growth rings. The fixed camera setup resulted in the  
377  
background constituting a non-negligible proportion of the images, especially for smaller  
378  
otoliths. This is especially true due to the curved or oval shape of the otolith, as a  
379  
compressed image will not only have less pixels to work with but will also have a  
380  
comparatively more important fraction of black background, which is effectively useless  
381  
for age interpretation. Otoliths of other fish species like red mullet which have a more  
382  
circular shape may be less sensitive to this problem (Politikos et al., 2021).  
383  
Improvements might therefore be made by instead first isolating the otoliths from their  
384  
background and cropping the image accordingly, in order to have a machine learning  
385  
network trained on using exclusively the information contained within the area of  
386  
interest. This would also limit information loss from image compression.  
387

## Outliers and transparency 388

The different networks were generally able to predict the age of otoliths with less than a  
389  
one-year deviation from the labelled values. It is noteworthy that predicted ages were  
390  
similar across different models and errors of more than a year were only seen in 2% of  
391  
the predictions on the test set. Closer inspection revealed that such errors were often  
392  
caused by otolith images with poor readability, in particular drastic changes in exposure  
393  
or visual damages and interruptions on the reading axis.  
394

Interestingly, for one of these images, the predicted age was correct, and a  
395  
reexamination by an expert revealed that the initial annotation was wrong by two years.  
396  
While the previous results suggest that the network may not have relied entirely on ring  
397  
patterns for estimating age, this correct prediction of a wrongly assigned age shows that  
398  
it is still utilizing cues that are somewhat age-specific. Model behaviour was also similar  
399

across all networks on single predictions of outliers: four were identified in all of the  
models, suggesting they must have learned the same features.  
400  
401

## Effects of image exposure on predictive power 402

Among the 17 models trained and explored in this study, models trained on  
low-exposure images gave the best performance. Models trained on the  
medium-exposure images and the nine-channel images also performed better than the  
high-exposure images. The reason for this is not entirely clear but has been observed in  
other studies. While low-exposure images may seem too dark and thereby hide useful  
visual details from a human point of view, our results show that it is not necessarily the  
case for an algorithm operating on finer-scale pixel values. It is likely that overexposure  
causes burnout and irreversible loss of information while underexposed images retain  
their information and only suffer from introduced noise.  
403  
404  
405  
406  
407  
408  
409  
410  
411

## Effects of 9-channel composite images and architecture size 412

Combining all 3 exposures into a 9-channel image did not perform better even if more  
information was available to these CNNs. The EfficientNetV2 models trained on these  
perform similarly to models trained on single-exposure images. The variance of  
predictions on 9-channel images was noticeably lower than for regular images, meaning  
the CNNs were more certain in their prediction even when the prediction was wrong.  
413  
414  
415  
416  
417

We also found that the newer and larger EfficientNetV2 architecture did not stand  
out as better than the EfficientNetV1 models. On the contrary, some of the best models  
were the smaller ones of B4, B5, and B6 (Table 4, Figure 3). This could be due to the  
size of our data set not being large enough to utilizing all the parameters in the larger  
models. Larger networks are generally able to better explore a larger data set, such as  
ImageNet, through training.  
418  
419  
420  
421  
422  
423

## Utilising model ensembles. 424

We observed slight improvements in performance when an ensemble of models was used  
for prediction. The use of numerous models in ensembles resulted in large numbers of  
combinations of model predictions with varying accuracy. Some combinations achieved  
425  
426  
427

higher accuracy than others (close to 79% for some combinations of six and seven  
428  
models). However, the mean ensemble prediction accuracy for a given number of models  
429  
showed that five models or more in combination resulted in accuracy just above 75%.  
430  
Five models thus seem to be sufficient and there could be minimal gain in precision in  
431  
combining larger numbers of models. Interestingly, ensembles combining models with  
432  
higher variance resulted in better predictions. This can indicate that if models are too  
433  
similar in individual predictions, the averaging effect ("wisdom of the crowds") will not  
434  
play out in the same way as when models with higher variance are combined.  
435  
Remarkably, many predictions only disagreed with a small decimal fraction. This could  
436  
imply that the models learned the same features in the otolith images.  
437

## Comparison of CNN with human readers

438

The comparison of age-specific percentage agreement in CNN-based predictions with  
439  
those from an internal age reading workshop shows that our models may achieve similar  
440  
agreement with human readers. While the numerical results are not directly comparable  
441  
in the sense that two different sets of otoliths were read, the trends in mean precision  
442  
across age groups were similar. Of particular interest is the fact that the mean  
443  
percentage agreement for our CNN-based predictions for a given age group generally fell  
444  
within or close to the range of percentage agreement for all otoliths of a given age class  
445  
seen between all readers involved in an age reading workshop. This may indicate that  
446  
while machine-based methods have not yet have the predictive accuracy of an expert  
447  
human reader, their estimates still fall within the expected range and may not be easily  
448  
distinguishable from those of traditional readers. Further testing should be conducted  
449  
to assess whether this is consistent, for example by conducting a multi-reader aging  
450  
event that includes undisclosed machine-based estimates of the same samples and  
451  
monitoring how they compare and whether they can be picked out by human readers.  
452

## Resource efficiency

453

Even if networks are reliable and trustworthy a remaining question will still be whether  
454  
there are significant cost benefits of deploying a ML framework for age reading of  
455  
otoliths. Despite fast progress, the results remain mixed and often yield lower precision  
456

and consistency than those obtained by trained expert readers, which limits the  
457 application of automated methods in real conditions. However, one aspect that is often  
458 under-considered by such studies is the practical time and cost benefits that  
459 implementing a functional ML framework would provide. As noted by Fisher and  
460 Hunter (2018) (Fisher and Hunter, 2018) in their review of digital techniques for otolith  
461 analysis, “costs for human and machine ageing systems are broadly similar since a large  
462 part of the cost is associated with preparing the otolith sections”. As such, the net  
463 benefit of automated ageing routines is directly dependent on the ability to scale  
464 performance using a comparatively smaller number of samples than expert readers or,  
465 alternatively, to train them on “rougher” data that can be produced faster and at a  
466 more efficient cost. Our study brings a net improvement toward this resource-efficient  
467 inclusion of machine-driven analysis to age reading, as our networks were trained  
468 exclusively on imaged broken otoliths. Whereas sectioned material requires time and  
469 laboratory resources to embed, section, and prepare the samples for imaging, breaking  
470 otoliths can be done immediately following collection from the fish. This means that  
471 images and age estimates could potentially be produced directly at sea, or at least  
472 processed in bulk as soon as the vessel and data are brought back to land.  
473

Also, CNNs can be applied without high additional cost or even be incorporated into  
474 the routine protocols, but add a new value e.g., reading consistency check, time-drift  
475 evaluations, inter-reader comparisons (how much ‘off’ is each reader when compared to  
476 the CNN predictions, even if not compared with the same otolith samples), etc. The  
477 advantages of ensemble predictions will also be easier to gain with networks. Ensembles  
478 of several expert readers are highly resource-demanding – especially when scaling to  
479 huge datasets – while an ensemble of, say eight versus three networks only requires a  
480 little bit more computation.  
481

We see the process of CNN implementation as an evolution of the protocols, with an  
482 intensive phase of model development and training. Through gradual improvement of  
483 model reliability, CNNs could emerge as a complementary supportive tool for traditional  
484 age estimations. The integration of those technologies could help scale the capacity of  
485 age reading experts and improve the sampling of biological data and monitoring of  
486 various fish stocks.  
487

While the exact features used by the networks may differ from those interpreted by  
488

human readers, one may be content with a trained network as a black box relying 489  
entirely on its empirical accuracy. Deep learning techniques are particularly powerful in 490  
detecting patterns in data (LeCun et al., 2015), and whether the networks actually 491  
detect and count annual increments as the defining features or not, a causal relationship 492  
between what the network attends to and the structure of the otoliths is likely. If the 493  
network does not use growth zones as the primary features for prediction, this means 494  
that it found useful correlating patterns unavailable or not obvious to the human eye. 495  
This was demonstrated in the case of Greenland halibut otoliths where the shape of the 496  
otoliths seemed to be the defining characteristic correlated with age (Ordonez et al., 497  
2020). Machine learning frameworks may therefore be used as complementary age 498  
readers to experts participating in otolith image interpretation workshops, as 499  
informative input playing part of additional background information, or relied upon as 500  
autonomous age readers without a subjective bias specific to increment identification 501  
and counting. As efforts to develop machine-assisted frameworks increase, an important 502  
question to ask is therefore whether they are to be trained at replicating human 503  
methodology for specific tasks or instead given the freedom to generate new and often 504  
not easily visualised methods. 505

## Conclusion 506

Our results demonstrate that the use of deep learning techniques in the analysis of 507  
otoliths have a major potential for facilitating automation. We believe that carefully 508  
trained CNNs could become a major component in automated pipelines that require 509  
minimal processing and could be able to produce near at sea age estimates. 510

When developing the CNN framework for the automatic age estimation, it is advised 511  
to include B4 architectures as they are quick to train, and performs good. Ensemble 512  
approaches can also be recommended if heavier computing effort is not detrimental to 513  
the automation process, as they could provide a more robust and higher-performing 514  
prediction. For a quick-to-train ensemble, B5 and Medium could be added. Those 515  
results also indicate that the use of slightly under-exposed images may be beneficial. 516

## Acknowledgements

517

We thank Jane Godiksen and age readers and technicians from the Demersal Fish  
518  
research group for providing otolith age estimates and images used for this study. We  
519  
thank Erlend Langhelle for providing insight into the image-taking-protocol and age  
520  
interpretation of cod otoliths.  
521

## References

522

- Abadi, M., Agarwal, A., Barham, P., Brevdo, E., Chen, Z., Citro, C., Corrado, G. S.,  
523  
Davis, A., Dean, J., Devin, M., et al. (2016). Tensorflow: Large-scale machine  
524  
learning on heterogeneous distributed systems. *arXiv preprint arXiv:1603.04467.*  
525
- Albuquerque, C. Q., Lopes, L. C. S., Jaureguizar, A. J., and Condini, M. V. (2019).  
526  
The visual quality of annual growth increments in fish otoliths increases with latitude.  
527  
*Fisheries Research*, 220: 105351.  
528
- Beamish, R. J. and McFarlane, G. A. (1995). A discussion of the importance of aging  
529  
errors, and an application to walleye pollock: the world's largest fishery. in recent  
530  
developments in fish otolith research. *University of South Carolina Press, Columbia,*  
531  
*S.C.*, pp. 545–565.  
532
- Brunel, T. and Piet, G. J. (2013). Is age structure a relevant criterion for the health of  
533  
fish stocks? *ICES Journal of Marine Science*, 70: 270–283.  
534
- Campana, S. (2001). Accuracy, precision and quality control in age determination,  
535  
including a review of the use and abuse of age validation methods. *Journal of fish  
536  
biology*, 59(2):197–242.  
537
- Carbonara, P. and Follesa, M. C. (2019). Handbook on fish age determination: a  
538  
mediterranean experience. *General Fisheries Commission for the Mediterranean.  
539  
Studies and Reviews*, 98: 1–179.  
540
- Chollet, F. and others (2018). Keras 2.1.3. <https://github.com/fchollet/keras>.  
541
- Denechaud, C., Smoliński, S., Geffen, A. J., Godiksen, J. A., and Campana, S. E.  
542

- (2020). A century of fish growth in relation to climate change, population dynamics and exploitation. *Global Change Biology*, 26(10):5661–5678. 543
- Fisher, M. and Hunter, E. (2018). Digital imaging techniques in otolith data capture, analysis and interpretation. *Marine Ecology Progress Series*, 598: 213–231. 545
- Francis, R. C. and Campana, S. E. (2011). Inferring age from otolith measurements: a review and a new approach. *Canadian Journal of Fisheries and Aquatic Sciences*. 547  
*NRC Research Press Ottawa, Canada.* 548
- <https://cdnsciencepub.com/doi/abs/10.1139/f04-063> (Accessed 3 February 2022). 549
- Froese, R. and Pauly, D. (2022). Fishbase. 550
- Hidalgo, M., Rouyer, T., Molinero, J. C., Massutí, E., Moranta, J., Guijarro, B., , and Stenseth, N. C. (2011). Synergistic effects of fishing-induced demographic changes and climate variation on fish population dynamics. *Marine Ecology Progress Series*, 426: 1–12. 552
- Høie, H., Millner, R. S., McCully, S., Nedreaas, K. H., Pilling, G. M., and Skadal, J. (2009). Latitudinal differences in the timing of otolith growth: A comparison between the barents sea and southern north sea. *Fisheries Research*, 96: 319–322. 556
- Krizhevsky, A., Sutskever, I., and Hinton, G. E. (2012). ImageNet Classification with Deep Convolutional Neural Networks. In Pereira, F., Burges, C. J. C., Bottou, L., and Weinberger, K. Q., editors, *Advances in Neural Information Processing Systems 25*, pages 1097–1105. Curran Associates, Inc. 559
- LeCun, Y., Bengio, Y., and Hinton, G. (2015). Deep learning. *Nature*, 563  
521(7553):436–444. 564
- Loshchilov, I. and Hutter, F. (2016). Sgdr: Stochastic gradient descent with warm restarts. *neurips*. 565
- Mahé, K. (2009). Project no. 044132. *Automated FISH Ageing (AFISA): final activity report*. 567
- Mingxing Tan and, Q. V. L. (2021). Efficientnetv2: Smaller models and faster training. *CoRR*, abs/2104.00298. 569

- Moen, E., Handegard, N. O., Allken, V., Albert, O. T., Harbitz, A., and Malde, K. (2018). Automatic interpretation of otoliths using deep learning. *PLoS ONE*. 571
- Myers, S., Thorsen, A., Godiksen, J., Malde, K., and Handegard, N. (2019). An efficient 573 protocol and data set for automated otolith image analysis. *GeoScience Data Journal*. 574
- Ordonez, A., Eikvil, L., Salberg, A.-B., Harbitz, A., Murray, S. M., and Kampffmeyer, 575 M. C. (2020). Explaining decisions of deep neural networks used for fish age 576 prediction. *PLoS ONE*, 15(6):e0235013. 577
- Panfili, J., de Pontual, H., Troadec, H., and Wrigg, P. J. (2002). Manual of fish 578 sclerochronology. <https://archimer.ifremer.fr/doc/00017/12801/> (Accessed 3 579 February 2022). 580
- Paszke, A., Gross, S., Massa, F., Lerer, A., Bradbury, J., Chanan, G., Killeen, T., Lin, 581 Z., Gimelshein, N., Antiga, L., Desmaison, A., Kopf, A., Yang, E., DeVito, Z., Raison, 582 M., Tejani, A., Chilamkurthy, S., Steiner, B., Fang, L., Bai, J., and Chintala, S. 583 (2019). Pytorch: An imperative style, high-performance deep learning library. In 584 Wallach, H., Larochelle, H., Beygelzimer, A., d'Alché-Buc, F., Fox, E., and Garnett, 585 R., editors, *Advances in Neural Information Processing Systems 32*, pages 8024–8035. 586 Curran Associates, Inc. 587
- Politikos, D. V., Petasis, G., Chatzispyrou, A., Mytilineou, C., and Anastasopoulou, A. 588 (2021). Automating fish age estimation combining otolith images and deep learning: 589 The role of multitask learning. *Fisheries Research*, 242: 106033. 590
- Ragonese, S. (2018). Methuselah or butterfly? when fish age estimates and validations 591 tell different stories. the case of the european hake (*merluccius merluccius* l. 1758) in 592 the mediterranean sea. ””. 593
- Reglero, P. and Mosegaard, H. (2006). Onset of maturity and cohort composition at 594 spawning of baltic sprat *sprattus sprattus* on the basis of otolith macrostructure 595 analysis. *Journal of Fish Biology*, 68: 1091–1106. 596
- Russakovsky, O., Deng, J., Su, H., Krause, J., Satheesh, S., Ma, S., Huang, Z., 597 Karpathy, A., Khosla, A., Bernstein, M., Berg, A. C., and Fei-Fei, L. (2014). 598 Imagenet large scale visual recognition challenge. 599

- Siskey, M. R., Wilberg, M. J., Allman, R. J., Barnett, B. K., and Secor, D. H. (2016).  
Forty years of fishing: changes in age structure and stock mixing in northwestern  
atlantic bluefin tuna (*thunnus thynnus*) associated with size-selective and long-term  
exploitation. *ICES Journal of Marine Science*, 73: 2518–2528.  
Smoliński, S., Deplanque-Lasserre, J., Hjörleifsson, E., Geffen, A. J., Godiksen, J. A.,  
and Campana, S. E. (2020). Century-long cod otolith biochronology reveals  
individual growth plasticity in response to temperature. *Scientific reports*, 10(1):1–13.  
Szegedy, C., Vanhoucke, V., Ioffe, S., Shlens, J., and Wojna, Z. (2015). Rethinking the  
inception architecture for computer vision. *CoRR*, abs/1512.00567.  
Tan, M. and Le, Q. V. (2019). Efficientnet: Rethinking model scaling for convolutional  
neural networks. *CoRR*, abs/1905.11946.  
Tyler, A. V., Beamish, R. J., and McFarlane, G. A. (1989). Implications of age  
determination errors to yield estimates. *ICES Journal of Marine Science*, 108: 27–35.  
Vabø, R., Moen, E., Smoliński, S., Åse Husebø, Handegard, N. O., and Malde, K.  
(2021). Automatic interpretation of salmon scales using deep learning. *Ecol. Inform.*  
63, 101322 (2021).  
Wightman, R. (2019). Pytorch image models.  
<https://github.com/rwightman/pytorch-image-models>.  
Xu, B., Wang, N., Chen, T., and Li, M. (2015). Empirical evaluation of rectified  
activations in convolutional network. *CoRR*, abs/1505.00853.  
Yosinski, J., Clune, J., Bengio, Y., and Lipson, H. (2014). How transferable are features  
in deep neural networks? In Ghahramani, Z., Welling, M., Cortes, C., Lawrence,  
N. D., and Weinberger, K. Q., editors, *Advances in Neural Information Processing  
Systems 27*, pages 3320–3328. Curran Associates, Inc.

# 1 Supplementary information

624

## 1.1 Hyper-parameters

625

**Table 3.** Hyper-parameters on each model

Param/CNN	B4	B5	B6	Medium	Large
<code>train_batch_size</code>	8	8	16	8	8
<code>img_size</code>	380	456	528	384	384
<code>val_img_size</code>	380	456	528	384	384
<code>steps_per_epoch</code>	1600	1600	1600	1600	1600
<code>epochs</code>	150	150	250	450	450
<code>early_stopping</code>	-	-	-	40	40
<code>early_stopping_patience</code>	14	14	22	-	-
<code>reduceLROnPlateau_patience</code>	7	7	11	-	-

Medium all-, and min-exposures was run with `steps_per_epoch`=160

B6 has `epochs`=150, `early_stopping_patience`=14, and `reduceLROnPlateau_patience`=7

B4 min was run with `img_size`=456

**Table 4.** Hyper-parameters on all models, TensorFlow only (B4,B5, B6), and PyTorch only (Medium and Large)

Parameter	Value	TensorFlow	PyTorch
<code>learning_rate</code>	1e-05	v	v
<code>n_fold</code>	10	v	v
<code>test_size</code>	0.1	v	v
<code>in_chans</code>	3 or 9	v	v
<code>reduceLROnPlateau_factor</code>	0.2	v	x
<code>which_exposure</code>	min, medium, max	v	x
<code>scheduler</code>	CosineAnnealingLR	x	v
<code>T_max</code>	10	x	v
<code>min_lr</code>	1e-06	x	v
<code>weight_decay</code>	1e-06	x	v
<code>which_exposure</code>	min, medium, max, all	x	v

`in_chans` is the number of channels as input for the model. It was either 3 for an RGB image or 9 channels for 3 images.

## 2 Descriptive Statistics

626

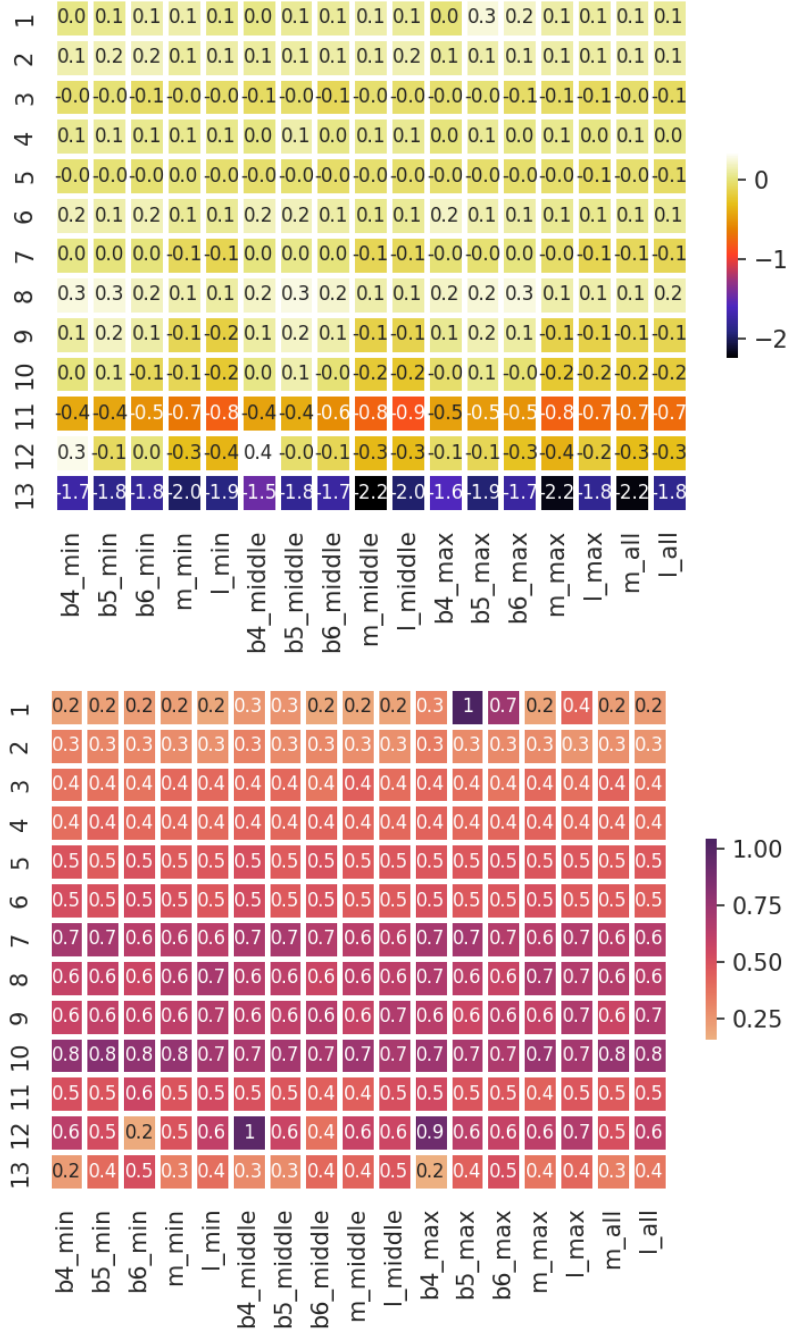


**Figure 8.** Model mean (top) and standard deviation (bottom) of residual test set prediction by age class

## 2.1 Model accuracy and MSE per fold

627

**Table 5.** MSE per CNN per fold

CNN/fold	1	2	3	4	5	6	7	8	9	10	ens.	Mean
B4,min	.320	.318	.306	.313	.322	.314	.315	.316	.306	.302	.277	.313
B4,middle	.344	.328	.316	.334	.326	.320	.355	.326	.313	.325	.285	.329
B4,max	.340	.317	.318	.347	.336	.336	.336	.320	.354	.336	.291	.334
B5,min	.324	.322	.325	.336	.291	.314	.320	.331	.33	.317	.277	.321
B5,middle	.308	.286	.315	.349	.332	.310	.280	.275	.331	.288	.273	.307
B5,max	.472	.302	.437	.459	.432	.366	.356	.441	.438	.418	.359	.412
B6,min	.325	.329	.334	.293	.312	.290	.320	.300	.276	.306	.272	.309
B6,middle	.323	.301	.312	.268	.294	.266	.309	.311	.278	.289	.262	.295
B6,max	.435	.306	.306	.270	.390	.321	.411	.321	.294	.448	.305	.350
m,min	.292	.292	.294	.275	.298	.304	.304	.331	.307	.295	.273	.299
m,middle	.287	.302	.307	.332	.288	.276	.277	.294	.304	.278	.278	.295
m,max	.337	.297	.302	.291	.315	.347	.338	.321	.313	.283	.289	.314
m,all	.289	.299	.303	.284	.292	.287	.303	.288	.289	.294	.273	.293
l,min	.267	.316	.269	.270	.322	.332	.280	.307	.303	.299	.280	.297
l,middle	.300	.332	.320	.300	.272	.302	.294	.285	.307	.285	.275	.300
l,max	.322	.295	.324	.353	.295	.306	.271	.292	.380	.299	.286	.314
l,all	.285	.293	.283	.274	.286	.325	.272	.283	.277	.295	.271	.287
Mean	.328	.308	.316	.315	.318	.313	.314	.314	.318	.315	.284	.316

628

**Table 6.** Accuracy per CNN per fold

CNN/fold	1	2	3	4	5	6	7	8	9	10	ens.	Mean
B4, min	69.9	68.9	68.7	68.3	68.9	70.1	69.7	66.8	68.9	72.4	72.8	69.3
B4, middle	68.5	69.3	73.0	68.5	67.8	68.2	67.2	67.2	68.3	69.5	71.5	68.8
B4, max	64.1	68.2	67.2	66.2	67.8	69.5	67.2	69.3	66.2	65.2	70.9	67.1
B5, min	71.8	69.1	69.3	66.8	73.6	70.7	66.2	68.3	69.5	68.7	74.4	69.4
B5, middle	70.3	72.0	67.8	66.6	67.4	69.9	71.8	71.5	68.2	72.2	73.4	69.8
B5, max	71.3	71.1	67.4	73.2	66.4	68.9	64.1	69.1	68.7	71.8	73.2	69.2
B6, min	68.3	68.5	66.4	72.4	70.7	70.9	69.3	69.3	72.0	68.9	73.4	69.7
B6, middle	68.5	69.9	67.6	73.6	72.8	72.0	68.0	69.3	72.0	71.1	74.4	70.5
B6, max	70.5	68.2	65.2	73.2	69.1	67.8	68.0	68.0	72.8	68.5	71.5	69.1
m, min	71.1	71.1	69.5	73.4	71.8	70.9	70.9	69.7	70.1	71.5	74.0	71.0
m, middle	71.3	70.1	70.1	70.9	71.7	71.8	72.0	71.3	69.3	71.8	72.4	71.0
m, max	68.9	70.1	70.3	71.3	70.7	68.5	69.7	68.0	69.1	71.8	71.3	69.8
m, all	71.7	70.7	69.3	71.3	71.8	71.8	71.3	71.7	71.1	70.7	74.0	71.1
l, min	72.4	69.7	71.5	70.8	71.3	71.3	70.9	69.9	71.1	70.5	72.0	71.0
l, middle	68.7	68.0	69.7	71.8	71.1	71.1	69.7	70.5	71.1	72.0	72.8	70.4
l, max	71.1	70.1	69.9	74.2	72.8	71.1	72.2	71.1	71.1	70.1	72.4	71.4
l, all	71.8	71.7	71.8	71.7	71.7	68.0	73.2	71.7	73.0	71.5	72.2	71.6
Mean	70.0	69.8	69.1	70.8	70.4	70.1	69.5	69.6	70.1	70.5	72.7	70.0

629

## 2.2 Predicted age class for all models and ground truth

630

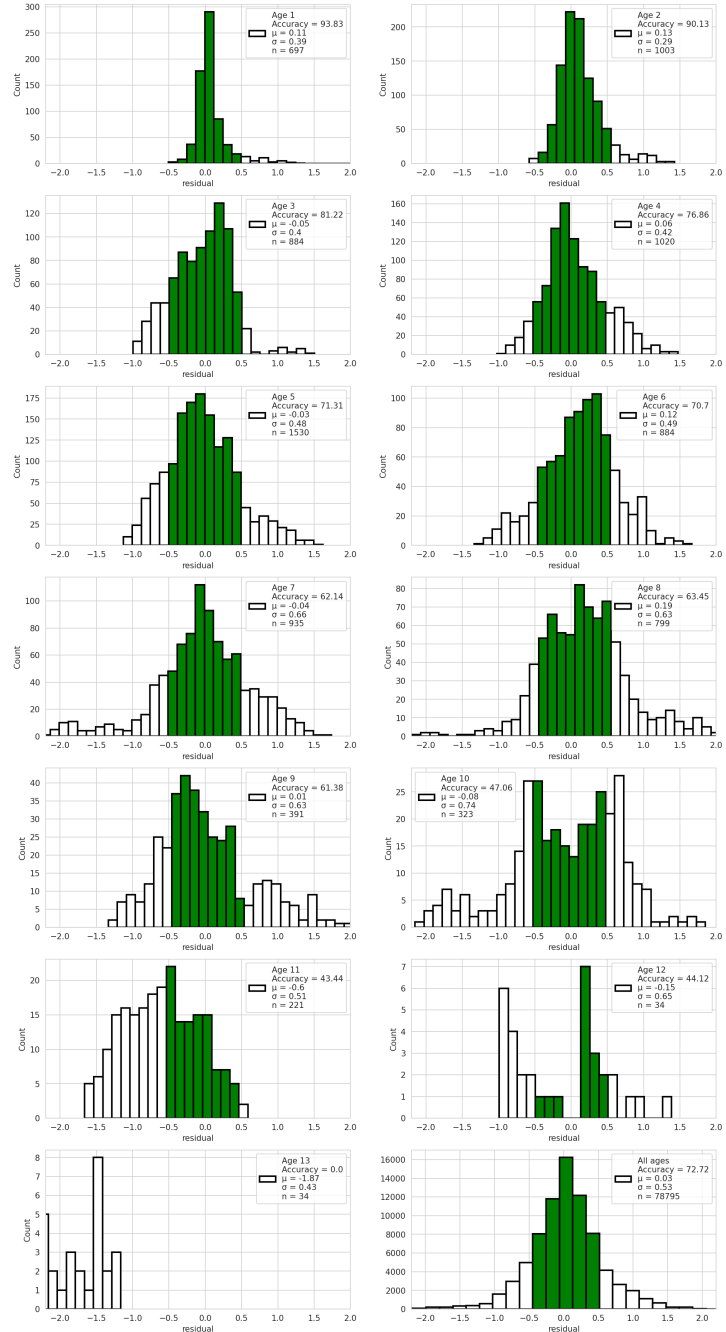


**Figure 9.** Predictions by age class from the average of all models. The green region shows the correctly classified age after rounding. The axis is fixed, hence outliers that differ from the true age by more than two years will not be visible.

### 3 Outliers

631

**Table 7.** Predictions error with residual of more than 1.5 years per model per index in test-set

Idx	13	17	47	48	71	92	154	270	279	308	312	320	334	342	362	369	393	418	423	444	462	481	502	Count
B4-min	9.8			5.1		11.7	9.9		5.5		11.1	5.1	8.2										8	
B4-mid	9.7			5.4		10.2			5.4	7.5	11.3	4.9	8.3	10.6	9.5								10	
B4-max	9.6			5.0		10.4					11.3	5.0	8.2										6	
B5-min	9.6			4.8		11.7	9.7				10.8	5.3						11.0					7	
B5-mid	9.8			6.7	11.5	11.8	9.8			10.9	5.3	8.4											9	
B5-max	9.8			4.5	11.5	9.6	7.7			10.6	5.1	8.3											8*	
B6-min	9.7			7.6	5.1	9.7				10.7	5.2	7.9	10.8	10.7									9	
B6-mid	9.6			5.1		11.5	9.7			10.8	5.2	8.3	10.8										9	
B6-max	9.8			5.2			5.7			10.7	5.2	8.2	10.6					6.5					9	
m-min		5.0	11.3		10.0					10.7	5.0	8.2					6.0						7	
m-mid		4.9	11.2		10.0					10.3	5.1	8.2												6
m-max		6.5	5.1	11.2	8.7	10.2				10.5	5.1	8.1					6.3							9
m-all		5.0	11.2		10.1					10.5	5.3	8.2					6.2				8.4			8
l-min		5.1	11.5		9.8	9.3				10.7	5.2	8.3					5.1							8
l-mid		5.0			9.8	9.4	5.5			10.6	5.2	8.1	10.5				6.0							9
l-max		9.5			9.9	3.6	5.4			10.8	5.1	8.2					5.9				8.4			10
l-all		9.3			9.8					10.8	5.2	8.0	10.5				6.2				8.5			9
Age	8	8	6	7	13	7	10	8	1	11	7	6	13	7	10	9	11	8	11	5	10	11	-	
Count	9	2	1	1	17	7	1	4	16	3	2	2	17	17	6	2	7	2	1	3	3	3	141	
As pct	53	12	6	6	100	41	6	24	94	18	12	12	6	100	100	35	12	41	12	6	18	18	-	

632

**Table 8.** Comments on the most frequently mispredicted otolith images

Idx	Comment
13	Labeled 8 years, and read as 10 years by the B-models (EfficientNet). The quality of the exposures was good, but there was a lot of split rings in the middle.
71	Labeled 7 years, and read as 5 years by all models. The exposures was very bright on all three axis, and the dorsal axis had a break line, and the plane was out of focus.
279	Labeled as 8 years, and read as 10 years by almost all models except B6-max. The exposures was of good quality, but there was split rings in the middle.
308	Labeled as 1 year, and read as 8 years, 6 years and 4 years by B5-max, b6-max, and Large-max respectively. The exposures was of good quality and the predicted age is obviously wrong.
342	Labeled as 13 years, and read as 11 years by all models. The quality of the exposures was good. The inner section is dark on the ventral side, the distal side is light, and the dorsal side has a break line. <small>633</small>
362	Labeled as 7 years, and read as 5 years by all models. This image is mislabeled. The otolith is obviously 5 years old.
369	Labeled as 10 years, and read as 8 years by all models except B5-min. The quality of the exposures was good, but it had split rings in the middle on bright exposures, and the contrast is strong.
393	Labeled as 9 years, and was read as 11 years by B4-middle, all B6 exposures and Large-middle and -all. The middle and min exposures was too dark. Max exposure was nice.
423	Labeled as 8 years, and read as 6 years by all the EfficientNetV2 models except Medium-middle. The quality of the images was bad. All the exposures was over-exposed. <small>634</small>

## 4 Ensembles by simple average

635

Table 10 shows the number of combinations of models that exist of tuples, triplets, and so on labeled with the heading "Coeff", then the best ensemble-average accuracy on the given number of combinations, and then the model numbers that produced the best combinations. Model number can be translated to model name using table 9. Table 11 shows the same information but selected to minimize MSE.

636

637

638

639

640

**Table 9.** The table shows the model family as columns and image exposure as rows. The numbering of models is used in reference to ensembles.

CNN family / Image exposure	EfficientNet			EfficientNetV2	
	B4	B5	B6	Medium	Large
Minimum	1	2	3	4	5
Medium	6	7	8	9	10
Maximum	11	12	13	14	15
9 channels	-	-	-	16	17

**Table 10.** Binomial combinations of simple average of ensembles accuracy

Coeff	#Comb	Best	Mean	Ensemble (see table 9)
2	136	75.9	74.1	(2, 5)
3	680	77.5	74.6	(1, 3, 4)
4	2380	77.9	74.9	(1, 2, 3, 4)
5	6188	77.9	75.1	(1, 2, 3, 4, 11)
6	12376	78.6	75.2	(1, 2, 3, 4, 8, 11)
7	19448	78.1	75.2	(1, 2, 3, 4, 7, 8, 11)
8	24310	77.5	75.2	(1, 2, 3, 4, 7, 8, 10, 11)
9	24310	77.5	75.3	(1, 2, 3, 6, 7, 8, 9, 11, 17)
10	19448	77.1	75.2	(1, 2, 3, 6, 7, 8, 9, 10, 12, 13)
11	12376	76.9	75.2	(1, 2, 3, 4, 6, 7, 8, 10, 11, 13, 16)
12	6188	76.7	75.2	(1, 3, 4, 7, 8, 10, 11, 13, 14, 15, 16, 17)
13	2380	76.3	75.1	(1, 3, 4, 7, 8, 9, 10, 11, 13, 14, 15, 16, 17)
14	680	75.9	75.1	(1, 2, 3, 4, 5, 8, 9, 10, 11, 12, 13, 14, 16, 17)
15	136	75.7	75.0	(1, 2, 3, 4, 5, 7, 8, 9, 10, 12, 13, 14, 15, 16, 17)
16	17	75.5	75.0	(1, 2, 3, 4, 5, 6, 7, 8, 9, 10, 12, 13, 14, 15, 16, 17)
17	1	74.8	74.8	(1, 2, 3, 4, 5, 6, 7, 8, 9, 10, 11, 12, 13, 14, 15, 16, 17)

641

642

643

**Table 11.** Binomial combinations of simple average of ensembles MSE

Coeff	#comb	best	Mean	Ensemble (see table 9)
2	136	0.250	0.265	(3, 17)
3	680	0.246	0.259	(1, 3, 5)
4	2380	0.245	0.256	(1, 3, 5, 7)
5	6188	0.245	0.254	(1, 3, 4, 7, 17)
6	12376	0.244	0.252	(1, 2, 3, 5, 8, 16)
7	19448	0.244	0.251	(1, 2, 3, 4, 5, 8, 11)
8	24310	0.244	0.251	(1, 2, 3, 4, 5, 8, 11, 17)
9	24310	0.244	0.250	(1, 2, 3, 4, 5, 7, 8, 11, 17)
10	19448	0.244	0.250	(1, 2, 3, 4, 5, 7, 8, 11, 16, 17)
11	12376	0.245	0.250	(1, 2, 3, 4, 5, 7, 8, 10, 11, 13, 16)
12	6188	0.245	0.249	(1, 2, 3, 4, 5, 6, 7, 8, 10, 11, 16, 17)
13	2380	0.245	0.249	(1, 2, 3, 4, 5, 6, 7, 8, 10, 11, 13, 16, 17)
14	680	0.245	0.249	(1, 2, 3, 4, 5, 6, 7, 8, 9, 10, 11, 13, 16, 17)
15	136	0.246	0.249	(1, 2, 3, 4, 5, 6, 7, 8, 9, 10, 11, 13, 15, 16, 17)
16	17	0.247	0.248	(1, 2, 3, 4, 5, 6, 7, 8, 9, 10, 11, 13, 14, 15, 16, 17)
17	1	0.248	0.248	(1, 2, 3, 4, 5, 6, 7, 8, 9, 10, 11, 12, 13, 14, 15, 16, 17)

**Table 12.** Comparison of the mean of all the 17 models (mean) with a total accuracy of 72.7% and the best ensemble model (Best Ens.) with a total accuracy of 78.6%. In all age groups, the ensemble improves on the mean-model accuracy except 13 year-olds.

Age	1	2	3	4	5	6	7	8	9	10	11	12	13
Mean	93.8	90.1	81.2	76.9	71.3	70.7	62.1	63.5	61.4	47.1	43.4	44.1	0
Best Ens.	95.1	93.2	84.6	80.0	78.9	78.9	65.6	76.6	69.6	52.6	61.5	50.0	0

#### 4.1 Pearson correlation of each model on test-set predictions

644

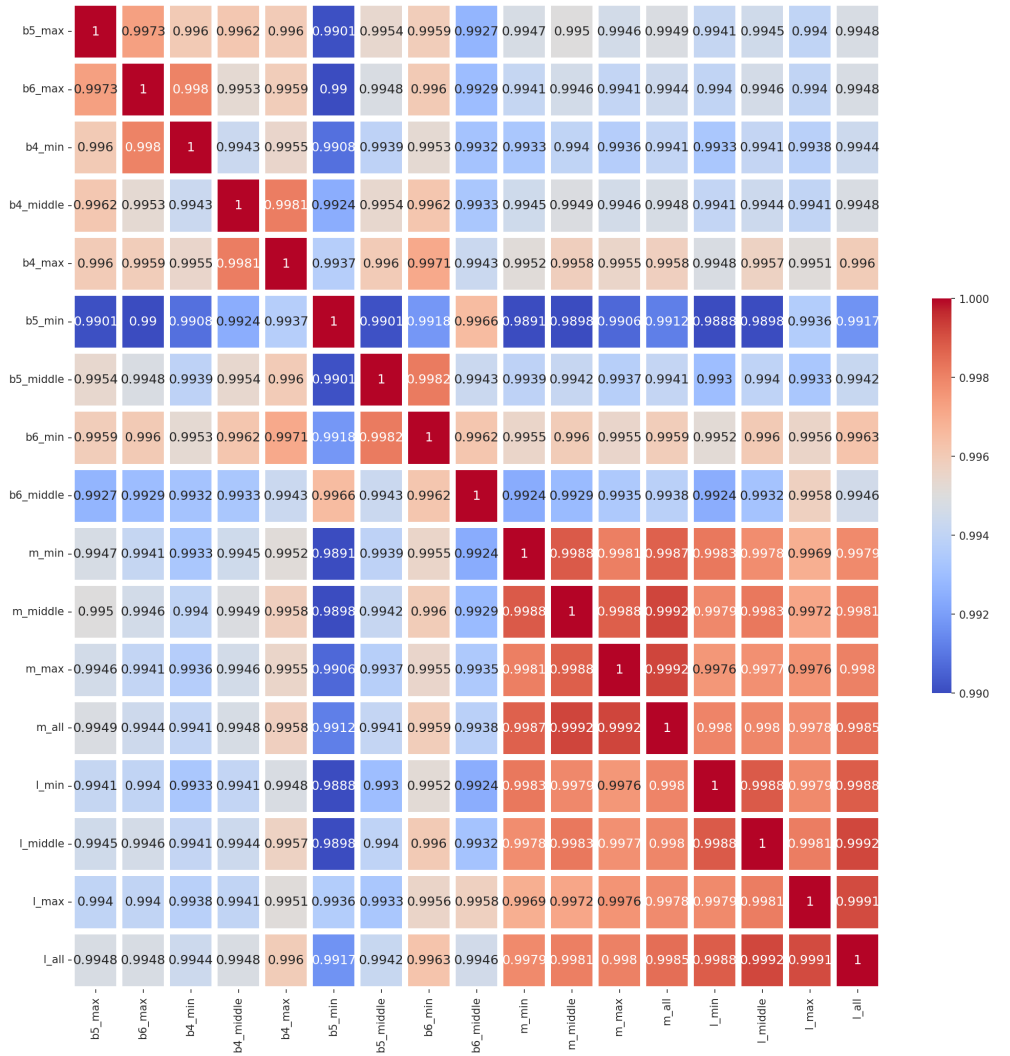


**Figure 10.** Pearson correlation of each model prediction on the test-set

#### 4.2 T-statistics of each model vs model comparison on test-set

645

#### prediction

646

**Table 13.** T-statistics of each model vs other models (order as in table 1)

no	2	3	4	5	6	7	8	9	10	11	12	13	14	15	16	17		
1	0.873	0.588	0.00901	0.0074	0.465	0.56	0.158	0.00554	0.0967	0.00645	0.938	0.864	0.361	0.00385	0.00322	0.00199		
2	-	0.768	0.0651	0.0679	0.462	0.723	0.284	0.0541	0.261	0.0173	0.851	0.782	0.601	0.0314	0.0407	0.0188		
3	-	-	0.0748	0.0755	0.251	0.931	0.381	0.0584	0.355	0.00417	0.649	0.566	0.826	0.0333	0.0408	0.0186		
4	-	-	-	-	-	0.86	0.00312	0.132	0.517	0.933	0.273	2.04E-05	0.0823	0.0467	0.0433	0.516	0.756	0.306
5	-	-	-	-	-	-	0.00293	0.139	0.562	0.764	0.282	2.65E-05	0.0875	0.0491	0.0348	0.381	0.546	0.205
6	-	-	-	-	-	-	-	0.256	0.0597	0.00219	0.0293	0.0414	0.6668	0.698	0.118	0.00138	0.00147	0.000743
7	-	-	-	-	-	-	-	-	0.46	0.111	0.46	0.00652	0.616	0.539	0.922	0.0646	0.084	0.0389
8	-	-	-	-	-	-	-	-	-	0.471	0.885	0.00104	0.26	0.199	0.422	0.289	0.388	0.189
9	-	-	-	-	-	-	-	-	-	-	0.213	1.78E-05	0.0725	0.0396	0.0259	0.532	0.8	0.306
10	-	-	-	-	-	-	-	-	-	-	-	0.000173	0.25	0.177	0.371	0.115	0.139	0.0611
11	-	-	-	-	-	-	-	-	-	-	-	-	0.0453	0.0007539	0.82E-061	0.58E-05	0.84E-06	-
12	-	-	-	-	-	-	-	-	-	-	-	-	-	0.514	0.0447	0.0586	0.0294	-
13	-	-	-	-	-	-	-	-	-	-	-	-	-	0.418	0.0234	0.0307	0.0145	-
14	-	-	-	-	-	-	-	-	-	-	-	-	-	-	0.0174	0.0134	0.00865	-
15	-	-	-	-	-	-	-	-	-	-	-	-	-	-	-	0.643	0.711	-
16	-	-	-	-	-	-	-	-	-	-	-	-	-	-	-	-	0.375	-